

Weakly-supervised Biomechanically-constrained CT/MRI Registration of the Spine

Bailiang Jian^{1,2}, Mohammad Farid Azampour¹[0000-0003-4077-1021], Francesca De Benetti^{1,2}[0000-0002-5255-4553], Johannes Oberreuter^{2,3}, Christina Bukas^{2,4}[0000-0001-9913-8525], Alexandra S. Gersing^{5,6}[0000-0003-1687-5541], Sarah C. Foreman^{5,6}[0000-0001-9140-0162], Anna-Sophia Dietrich^{5,6}, Jon Rischewski^{5,6}, Jan S. Kirschke^{5,6}[0000-0002-7557-0003], Nassir Navab^{1,7}[0000-0002-6032-5611], and Thomas Wendler^{1,2}[0000-0002-0915-0510]

- ¹ Chair for Computer Aided Medical Procedures and Augmented Reality, Technische Universität München, Garching, Germany, {bailiang.jian,wendler}@tum.de
² ScintHealth GmbH, Munich, Germany,
³ Reply SpA, Munich, Germany,
⁴ Helmholtz AI, Helmholtz Zentrum München, Munich, Germany,
⁵ Department of Radiology, Technische Universität München, Munich, Germany,
⁶ Department of Neuroradiology, Technische Universität München, Munich, Germany,
⁷ Computer Aided Medical Procedures Lab, Laboratory for Computational Sensing+Robotics, Johns Hopkins University, Baltimore, MD, USA

Abstract. Computed Tomography (CT) and Magnetic Resonance Imaging (MRI) are two of the most informative modalities in spinal diagnostics and treatment planning. CT is useful when analysing bony structures, while MRI gives information about the soft tissue. Thus, fusing the information of both modalities can be very beneficial. Registration is the first step for this fusion. While the soft tissues around the vertebra are deformable, each vertebral body is constrained to move rigidly. We propose a weakly-supervised deep learning framework that preserves the rigidity and the volume of each vertebra while maximizing the accuracy of the registration. To achieve this goal, we introduce anatomy-aware losses for training the network. We specifically design these losses to depend only on the CT label maps since automatic vertebra segmentation in CT gives more accurate results contrary to MRI. We evaluate our method on an in-house dataset of 167 patients. Our results show that adding the anatomy-aware losses increases the plausibility of the inferred transformation while keeping the accuracy untouched.

Keywords: CT/MRI registration · Deep learning image registration · Biomechanical constraints · Spine

1 Introduction

CT and MRI images are the most used imaging modalities for understanding the pathologies of the spine and defining the therapeutic approach. Experts need

both modalities for proper diagnosis in complex clinical situations as each modality provides different information [12]. CT has higher contrast in bony structures and is highly sensitive for fracture detection and other pathologies [19,27]. On the other hand, MRI can be used to detect lesions and tumors of the spinal cord and the intervertebral discs, as well as to evaluate the inner anatomy of the vertebral bodies [24]. As a result, registering spinal images from different modalities benefits various clinical contexts, ranging from improved diagnosis and proper treatment planning to personalized therapeutic decisions.

A major problem when registering articulated rigid structures is their relative motion and the soft tissue deformations due to patient movement. Indeed, rigid registration cannot address the problem of the varying curvature of patients' spine during different imaging sessions, as well as a global deformable registration ignores the difference between soft tissues and bony structures. Consequently, these general-purpose methods are not fully appropriate to solve our problem.

Few works have addressed the problem of rigid structures in conventional deformable registration. [14] and [4] defined a way to interpolate the deformations of rigid objects based on their euclidean distance transform (EDT). [2] proposed a poly-rigid/affine transformation model, which produces locally rigid/affine diffeomorphic deformation field. [15] and [26] imposed rigidity by introducing several constraints, including the linearity, orthonormality, and identity determinant of the transform matrix. [7] defined groups of springs between vertebrae and penalized the change in length of them. In addition, [13] penalized the inter-voxel distance change in rigid bodies. Finally, [21] proposed penalizing deviations of the Jacobian determinant of the deformation from unity to preserve the volume of lesions in breast MRI registration. [26] introduced the latter as one of the rigidity penalties in deformable registration, while proposing to use the orthonormality of a rigid transform as a rigidity penalty in registering digital subtraction angiography (DSA) images. However, these approaches are based on conventional iterative optimization methods, which are time-consuming, and their performance highly depends on the initialization and parameter settings. In more recent years, convolutional neural networks (CNNs) were used to do deep learning-based image registration (DLIR) [9]. Their main advantage is that they enable inferring a plausible transformation in a single iteration, using a model trained optimizing only image similarity and deformation smoothness [3,5,17]. A biomechanically-constrained method for DLIR of MRI-CT images of the prostate, proposed by [6], consists of training on finite element (FE) modeling-generated motion fields. However, it required the segmentation of the prostate in both modalities to establish the surface point cloud correspondence. This segmentation is non-trivial for the spine in MRI.

Another hurdle for unsupervised DLIR methods is the selection of the similarity metric for multi-modal image registration. For registration of MRI-CT of the pelvis, [18] introduced a new metric for unsupervised training of a deep network called self-correlation descriptor. [16] reduced the problem of MRI-CT registration of images of the neck to a mono-modal one by training a neural network to synthesize CT images from MRI. [11] proposed a weakly-supervised

framework that utilizes the Dice score (DSC) between the labels of the fixed image and the deformed moving image without any image-based similarity metrics during training. None of the above consider the rigidity of bony structures and the constraints that they impose on the deformation field. As a result, those registration results are not suitable for image fusion in the spine.

Our work introduces a weakly-supervised anatomy-aware method for registering spinal MR-CT images. We acknowledge that vertebrae segmentation is not a trivial task for MRI, thus we only rely on label maps from CT for training. Further, we devise losses and metrics to deal with the biomechanical constraints imposed by bony structures. Our main contributions are:

- Proposal of a framework for rigidity-preserving MRI/CT deformable registration of the spine taking rigidly aligned CT/MRI images as input
- Introduction of the rigid dice loss and rigid field loss for rigidity-preservation
- Adaptation of rigidity penalties used in conventional registration of spine to DLIR (orthonormal condition, properness condition)
- Extensive evaluation and ablation study of different losses on an in-house dataset with 167 patients

2 Method

Architecture Let $\mathcal{F} : \Omega_f \rightarrow \mathbb{R}$ denote the fixed image, and $\mathcal{M} : \Omega_m \rightarrow \mathbb{R}$ denote the moving image, where $\Omega_f \in \mathbb{R}^3$ and $\Omega_m \in \mathbb{R}^3$ represent the coordinate space of \mathcal{F} and \mathcal{M} . In our setup, the training loss consists of three terms. Firstly, the network learns to establish spatial correspondence between fixed and moving images by computing a dense deformation field (DDF) $\phi : \Omega_f \rightarrow \Omega_m$ through an intensity-based image similarity loss \mathcal{L}_{sim} . Second, a smoothness regularizer $\mathcal{L}_{\text{smooth}}$ ensures the output DDF is plausible and realistic. Lastly, we define rigidity penalties $\mathcal{L}_{\text{rigid}}$ between the moving label and the warped label, or on the deformation vectors inside the rigid bodies, to guarantee each of them is transformed rigidly. See their formal definition in the next subsections.

The network is trained by minimizing the following loss function:

$$\mathcal{L} = \mathcal{L}_{\text{sim}}(\mathcal{F}, \mathcal{M} \circ \phi) + \lambda_{\text{smooth}} \mathcal{L}_{\text{smooth}}(\mathbf{v}) + \lambda_{\text{rigid}} \sum_i^N \mathcal{L}_{\text{rigid}}(s_{\mathcal{M}}^i, s_{\mathcal{M}}^i \circ \phi, \phi) \quad (1)$$

where $\mathcal{M} \circ \phi : \Omega_f \rightarrow \mathbb{R}$ represents the warped moving image, $s_{\mathcal{M}}^i : \Omega_m \rightarrow \{0, 1\}$ is the binary segmentation label of the i th rigid body in the moving image, N is the number of rigid bodies, i.e., in our case, the vertebrae, and \mathbf{v} is the stationary velocity field (SVF) parameterizing the DDF ϕ . The smoothness regularizer $\mathcal{L}_{\text{smooth}}$ is computed as the l_2 -norm of the diffusion on the spatial gradient of the SVF \mathbf{v} .

We adopt the diffeomorphic version of VoxelMorph [3] as our baseline network. This 3D network architecture comprises a UNet [22] and two convolutional layers with 32 filters each to output the SVF \mathbf{v} . The UNet consists of an encoder with convolution filter channels [32, 32, 64, 64] and a decoder with channels

[64, 64, 64, 64]. To guarantee the invertibility and topology preservation, the predicted deformations are parameterized using the SVF under the Log-Euclidean framework. \mathbf{v} is integrated using the *scaling and squaring* method [1] with $T = 7$ time steps to obtain the diffeomorphic DDF ϕ [3].

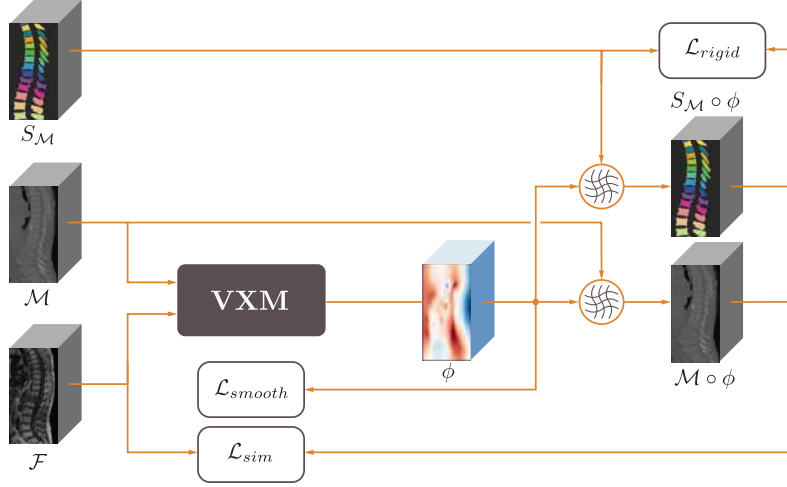


Fig. 1: An overview of the architecture: A VoxelMorph network (VXM) takes as input a CT as moving image \mathcal{M} , its label map $\mathcal{S}_{\mathcal{M}}$, and an MRI as fixed image \mathcal{F} . The output is a DDF ϕ . Three losses are applied on the warped CT (\mathcal{L}_{sim}), the warped label map (\mathcal{L}_{rigid}), and the DDF itself (\mathcal{L}_{smooth}).

Rigid dice loss To penalize structural changes on rigid parts, i.e. the vertebrae, we use a rigid dice loss. Let ϕ be the inferred deformation, then for each vertebra in the moving image (v_i) with binary segmentation label $s_{\mathcal{M}}^i$, we calculate the closest rigid transform ($T_{rigid}^{i,\phi}$) by solving the equation:

$$T_{rigid}^{i,\phi} = \underset{T_{rigid}}{\operatorname{argmin}} (s_{\mathcal{M}}^i \circ T_{rigid} - s_{\mathcal{M}}^i \circ \phi)^2. \quad (2)$$

Then the rigid dice loss for each vertebra can be defined as:

$$\mathcal{L}_{rigid}^{i \text{ dice}} = 1 - 2 * \frac{|(s_{\mathcal{M}}^i \circ T_{rigid}^{i,\phi}) \cap (s_{\mathcal{M}}^i \circ \phi)|}{|s_{\mathcal{M}}^i \circ T_{rigid}^{i,\phi}| + |s_{\mathcal{M}}^i \circ \phi|} \quad (3)$$

Rigid field loss To enforce a rigid transformation for each rigid body, we evaluate if the deformation field within the rigid body is close to a rigid deformation using the rigid field loss. Let $P_i = \{\mathbf{p}_j\}_{j=1,\dots,n}$, $\mathbf{p}_j \in s_{\mathcal{M}}^i$ be a set

of randomly selected points from i th vertebra (v_i) in the moving image and $Q_i = \{\mathbf{q}_j\}_{j=1,\dots,n}$, $\mathbf{q}_j \in s_{\mathcal{M}}^i \circ \phi$ the set of corresponding points to P_i in the warped image. Using P_i and Q_i , we can compute the average rigid transform for v_i (ϕ_{rigid}^i) by solving a least squares problem with singular value decomposition (SVD) [25]. Then, by minimizing the distance between the predicted deformation vectors and the average rigid transform vectors inside each vertebra, the network learns to move it rigidly (see also Supplementary Material).

$$\mathcal{L}_{\text{rigid field}}^i = \sum_{\mathbf{z} \in s_{\mathcal{M}}^i \circ \phi} (\phi_{\text{rigid}}^i(\mathbf{z}) - \phi(\mathbf{z}))^2 / |s_{\mathcal{M}}^i \circ \phi| \quad (4)$$

Properness condition We adapt the penalty of the determinant of the Jacobian proposed by [21] to the DLIR scenario and call it Properness condition (PC) as proposed by [26]. To implement it, first, we compute the ideal rotation matrix R of every voxel $\mathbf{z} \in \Omega_{\mathcal{F}}$ from the Jacobian of the DDF ϕ .

$$R(x) = J_{\phi}(x) \quad (5)$$

Then, we constrain the rotation matrices $R(x)$ of voxels inside each vertebra to have a proper unity determinant by minimizing the l_2 -distance between the Jacobian determinant and constant one:

$$\mathcal{L}_{\text{pc}} = \frac{1}{N} \sum_i^N \frac{1}{|s_{\mathcal{M}}^i \circ \phi|} \sum_{x \in s_{\mathcal{M}}^i \circ \phi} \|\det J_{\phi}(x) - 1\|_2^2 \quad (6)$$

Orthonormal condition We include the Orthonormal condition (OC) proposed by [26] in our setup, by computing the inner product of the Jacobian of the DDF J_{ϕ} and by penalizing the deviation of it from an identity matrix using the matrix norm. By forcing the rotation $R(x)$ of every voxel inside each vertebra to be orthonormal, the rigidity is preserved:

$$\mathcal{L}_{\text{oc}} = \frac{1}{N} \sum_i^N \frac{1}{|s_{\mathcal{M}}^i \circ \phi|} \sum_{x \in s_{\mathcal{M}}^i \circ \phi} \|J_{\phi}(x)^T J_{\phi}(x) - I\|_{\text{fro}}^2 \quad (7)$$

3 Experiments

Dataset We use an in-house dataset of 167 patients. The spatial resolution of the CTs ranges from (0.2, 0.2, 0.4) mm to (1.5, 1.5, 5) mm, while the T1-weighted MRIs have voxel spacing from (0.3, 0.3, 2.7) mm to (1, 1, 5) mm. The dataset has different fields of views and covers different part of spines, which in total, results in images of 1280 vertebrae. We split our dataset into training, validation and test sets with 117, 25 and 25 patients in each set, respectively. During training and inference, all images are resampled to 1 mm isotropic resolution, and the intensities are normalized to $[0, 1]$. Vertebra detection and segmentation

on CT images is done automatically using the framework of [23]. For MRI, an expert annotated the central point of each vertebra, and manually segmented the validation and test set. The vertebral central points of both modalities are used to rigidly register each image pair. The ground truth segmentation labels are used for measuring the registration accuracy in terms of DSC.

Hyperparameter tuning of image-similarity and smoothness We investigated three different multi-modal image similarity losses: normalized mutual information (NMI) [28], normalized gradient fields (NGF) [20,8], and a modality-independent neighbourhood descriptor (MIND)-based [10] loss. The MIND-based loss achieved the highest validation DSC. The hyperparameter λ_{smooth} was optimized with respect to the MIND-based similarity loss based on the validation set. Considering both the registration accuracy (given by the DSC) and the validity of the inferred transformation (given by the standard deviation (SD) of the logarithm of the Jacobian determinant, $\text{SD} \log |J_\phi|$), we find 0.01 to have the best performance so λ_{smooth} is fixed to 0.01 for the rest of the experiments. See validation results of the tuning in the Supplementary Material.

Ablation Studies To measure the effect of each loss we employed for rigidity, we perform an ablation study for each of them. First, we train our network without any rigidity penalties ($\lambda_{\text{rigid}} = 0$) for 500 epochs to get our baseline model. Then, starting from the milestone at 400 epochs, we add each of the rigidity penalties and train for another 100 epochs. We also compare our method with one conventional approach [26] (denoted as *Staring*), which takes NMI with OC and PC as loss function and iteratively optimizes for each pair of data.

Results Table 1 gives a detailed summary of our experiments (see Supplementary Material for weights setting). The baseline method performs better than the conventional *Staring* method, with 1.5% improvement in DSC and $100\times$ faster speed. However, it cannot guarantee the rigidity of the vertebrae and their volume drastically changes during registration. Our proposed anatomy-aware losses alleviate this issue. Specifically, \mathcal{L}_{pc} contributes significantly to the volume preservation, with only 4.8% loss per vertebra (Fig. 3). The $\mathcal{L}_{\text{rigid dice}}$, $\mathcal{L}_{\text{rigid field}}$ and \mathcal{L}_{oc} attain higher rigid dice than the baseline method, among which the rigid dice loss achieves the highest level of rigidity, with 5.7% improvement over the baseline. The combinations of PC and other penalties reduce the volume loss while maintaining the rigidity of the vertebrae, and yielding plausible and smooth DDF. Fig. 2 shows the boxplots of our experiments. The outliers are the cases where the boundary vertebrae are incomplete in CT/MRI images. With comparable registration accuracy, the proposed anatomy-aware losses significantly preserve the volume and rigid properties of the vertebrae. Qualitative results of the different methods are displayed in Fig. 3, where the red circles are showing regions of incorrect warped labels, while the greens outline correct

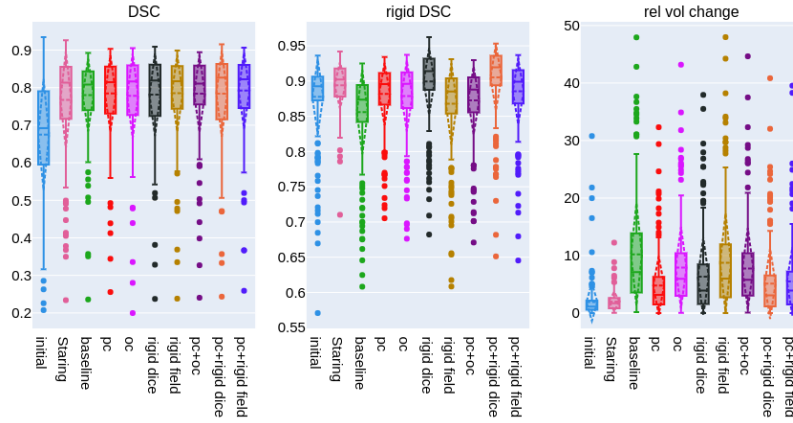


Fig. 2: Boxplots depicting the DSC, rigid dice and relative volume change $\% \Delta \text{vol}$ of initial dataset, conventional method, baseline and each loss setting.

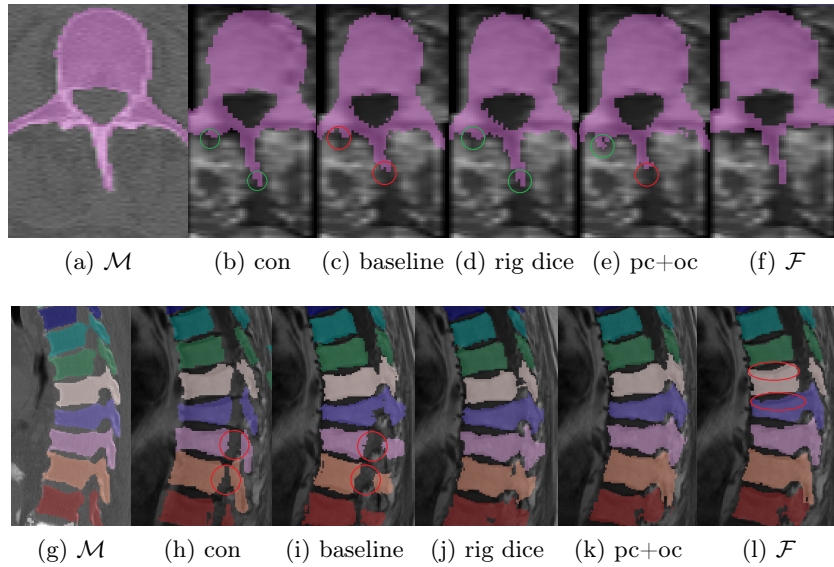


Fig. 3: Example axial (top) and sagittal (bottom) slices of moving image CT, fixed image superimposed by warped label from conventional, baseline, and other methods with different rigidity penalties.

ones. In particular, the axial views show that training with rigid dice loss help maintain the details in the process area. The sagittal views validate that the PC

preserves the volume, and the OC results in sharper borders. As shown in the axial slices, the incomplete transverse processes in MR images limit our method from getting high rigid DSC, since the network cannot predict missing parts.

PC during inference Finally, to validate PC’s effectiveness in volume preservation, we compare its performance with the direct volume loss, which tries to penalize the volume change before and after the registration directly. We also compute PC as a metric (lower is better), during inference (see Supplementary Material). With a similar $\% \Delta \text{vol}$, the direct volume loss gets a higher PC than training with PC in the test set. It indicates that PC preserves the volume in a more realistic way, without any compression or expansion in compensation. Moreover, training with OC can also decrease PC, which implies that enforcing the orthonormality of the transformation also contributes to unity determinant.

Table 1: Quantitative summary of the test set results given as averages(SD). DSC indicates the mean Dice score over all vertebrae. Similar to $\mathcal{L}_{\text{rigid dice}}$ (Sec 2), rigid DSC computes the DSC between the warped label $s_{\mathcal{M}}^i \circ \phi$ and the rigidly transformed label $s_{\mathcal{M}}^i \circ T_{\text{rigid}}^i$, to measure the level of rigidity kept during registration. $\% \Delta \text{vol}$ represents the relative volume change of each vertebra between source label $s_{\mathcal{M}}^i$ and warped label $s_{\mathcal{M}}^i \circ \phi$. To assess the plausibility of the inferred transformation, $|J_{\phi}|_{\leq 0}$ indicates the number of folding voxels in the DDF (less is better), $\text{SD} \log |J_{\phi}|$ measures the smoothness of the DDF (lower is better). The runtime is measured with CPU and with second as unit.

Method	DSC	Rigid DSC	$\% \Delta \text{vol}$	$ J_{\phi} _{\leq 0}$	$\text{SD} \log J_{\phi} $	Time
Initial	0.67(0.15)	0.88(0.05)	4.16(3.95)	-	-	-
Staring	0.77(0.13)	0.89(0.03)	2.02(1.65)	0	0.04(0.01)	243
Our baseline	0.78(0.10)	0.86(0.06)	10.21(8.91)	0.04(0.20)	0.13(0.05)	3.5(1.3)
pc	0.78(0.10)	0.88(0.04)	4.80(5.08)	1.60(7.84)	0.12(0.05)	3.7(1.2)
oc	0.78(0.11)	0.88(0.05)	7.90(7.09)	0.12(0.59)	0.13(0.05)	3.4(1.1)
rigid dice	0.78(0.12)	0.90(0.5)	6.32(6.77)	0.64(3.14)	0.13(0.05)	3.3(1.1)
rigid field	0.79(0.10)	0.87(0.06)	8.74(8.59)	0.08(0.39)	0.13(0.05)	3.6(1.2)
pc+oc	0.78(0.10)	0.87(0.05)	7.73(7.08)	0	0.12(0.05)	4.0(1.3)
pc+rigid dice	0.78(0.11)	0.90(0.05)	5.12(6.13)	18.30(63.20)	0.13(0.06)	3.4(1.1)
pc+rigid field	0.79(0.10)	0.89(0.05)	5.51(5.94)	2.40(11.80)	0.13(0.06)	3.6(1.2)

4 Conclusion

In this paper, we present a framework for rigidity- and volume- preserving deformable registration of spinal CT/MRI. Compared to supervised DLIR methods

which need both labels of the fixed and moving images, our approach only requires the moving label. We define two novel rigidity penalties (rigid dice loss and rigid field loss) to constrain the movement of the vertebrae. Moreover, we introduce PC and OC to the DLIR scenario. The results of extensive experiments indicate that PC is competent in volume preservation while the other three penalties guarantee the rigid properties of the vertebrae during deformable registration. Compared to conventional methods, our algorithm achieves higher accuracy and is significantly faster. Moreover, the proposed penalties can be easily transferred to other DLIR methods.

References

1. Arsigny, V., Commowick, O., Pennec, X., Ayache, N.: A log-euclidean framework for statistics on diffeomorphisms. In: International Conference on Medical Image Computing and Computer-Assisted Intervention. pp. 924–931. Springer (2006)
2. Arsigny, V., Pennec, X., Ayache, N.: Polyrigid and polyaffine transformations: a novel geometrical tool to deal with non-rigid deformations—application to the registration of histological slices. *Medical image analysis* **9**(6), 507–523 (2005)
3. Balakrishnan, G., Zhao, A., Sabuncu, M.R., Guttag, J., Dalca, A.V.: Voxelmorph: a learning framework for deformable medical image registration. *IEEE transactions on medical imaging* **38**(8), 1788–1800 (2019)
4. Bukas, C., Jian, B., Venegas, L.F.R., De Benetti, F., Ruehling, S., Sekuboyina, A., Gempt, J., Kirschke, J.S., Piraud, M., Oberreuter, J., et al.: Patient-specific virtual spine straightening and vertebra inpainting: An automatic framework for osteoplasty planning. In: International Conference on Medical Image Computing and Computer-Assisted Intervention. Springer (2021)
5. De Vos, B.D., Berendsen, F.F., Viergever, M.A., Sokooti, H., Staring, M., Išgum, I.: A deep learning framework for unsupervised affine and deformable image registration. *Medical image analysis* **52**, 128–143 (2019)
6. Fu, Y., Wang, T., Lei, Y., Patel, P., Jani, A.B., Curran, W.J., Liu, T., Yang, X.: Deformable mr-cbct prostate registration using biomechanically constrained deep learning networks. *Medical physics* **48**(1), 253–263 (2021)
7. Gill, S., Abolmaesumi, P., Fichtinger, G., Boisvert, J., Pichora, D., Borshneck, D., Mousavi, P.: Biomechanically constrained groupwise ultrasound to ct registration of the lumbar spine. *Medical image analysis* **16**(3), 662–674 (2012)
8. Haber, E., Modersitzki, J.: Intensity gradient based registration and fusion of multi-modal images. In: International Conference on Medical Image Computing and Computer-Assisted Intervention. pp. 726–733. Springer (2006)
9. Haskins, G., Kruger, U., Yan, P.: Deep learning in medical image registration: a survey. *Machine Vision and Applications* **31**(1), 1–18 (2020)
10. Heinrich, M.P., Jenkinson, M., Papież, B.W., Brady, S.M., Schnabel, J.A.: Towards realtime multimodal fusion for image-guided interventions using self-similarities. In: International conference on medical image computing and computer-assisted intervention. pp. 187–194. Springer (2013)
11. Hu, Y., Modat, M., Gibson, E., Li, W., Ghavami, N., Bonmati, E., Wang, G., Bandula, S., Moore, C.M., Emberton, M., et al.: Weakly-supervised convolutional neural networks for multimodal image registration. *Medical image analysis* **49**, 1–13 (2018)

12. Kim, G.U., Chang, M.C., Kim, T.U., Lee, G.W.: Diagnostic modality in spine disease: a review. *Asian Spine Journal* **14**(6), 910 (2020)
13. Kim, J., Matuszak, M.M., Saitou, K., Balter, J.M.: Distance-preserving rigidity penalty on deformable image registration of multiple skeletal components in the neck. *Medical physics* **40**(12), 121907 (2013)
14. Little, J.A., Hill, D.L., Hawkes, D.J.: Deformations incorporating rigid structures. *Computer Vision and Image Understanding* **66**(2), 223–232 (1997)
15. Loeckx, D., Maes, F., Vandermeulen, D., Suetens, P.: Nonrigid image registration using free-form deformations with a local rigidity constraint. In: *International Conference on Medical Image Computing and Computer-Assisted Intervention*. pp. 639–646. Springer (2004)
16. McKenzie, E.M., Santhanam, A., Ruan, D., O’Connor, D., Cao, M., Sheng, K.: Multimodality image registration in the head-and-neck using a deep learning-derived synthetic ct as a bridge. *Medical physics* **47**(3), 1094–1104 (2020)
17. Mok, T.C., Chung, A.: Conditional deformable image registration with convolutional neural network. In: *International Conference on Medical Image Computing and Computer-Assisted Intervention*. pp. 35–45. Springer (2021)
18. Momin, S., Lei, Y., Wang, T., Fu, Y., Patel, P., Jani, A.B., Curran, W.J., Liu, T., Yang, X.: Ct-mri pelvic deformable registration via deep learning. In: *Medical Imaging 2021: Image-Guided Procedures, Robotic Interventions, and Modeling*. vol. 11598, p. 1159818. International Society for Optics and Photonics (2021)
19. Parizel, P., Van Der Zijden, T., Gaudino, S., Spaepen, M., Voormolen, M., Ventermans, C., De Belder, F., Van Den Hauwe, L., Van Goethem, J.: Trauma of the spine and spinal cord: imaging strategies. *European Spine Journal* **19**(1), 8–17 (2010)
20. Pluim, J.P., Maintz, J.A., Viergever, M.A.: Image registration by maximization of combined mutual information and gradient information. In: *International Conference on Medical Image Computing and Computer-Assisted Intervention*. pp. 452–461. Springer (2000)
21. Rohlfing, T., Maurer, C.R., Bluemke, D.A., Jacobs, M.A.: Volume-preserving non-rigid registration of mr breast images using free-form deformation with an incompressibility constraint. *IEEE transactions on medical imaging* **22**(6), 730–741 (2003)
22. Ronneberger, O., Fischer, P., Brox, T.: U-net: Convolutional networks for biomedical image segmentation. In: *International Conference on Medical image computing and computer-assisted intervention*. pp. 234–241. Springer (2015)
23. Sekuboyina, A., Rempfler, M., Kukačka, J., Tetteh, G., Valentinitzsch, A., Kirschke, J.S., Menze, B.H.: Btrfly net: Vertebrae labelling with energy-based adversarial learning of local spine prior. In: *International Conference on Medical Image Computing and Computer-Assisted Intervention*. pp. 649–657. Springer (2018)
24. Shah, L.M., Salzman, K.L.: Imaging of spinal metastatic disease. *International journal of surgical oncology* **2011** (2011)
25. Sorkine-Hornung, O., Rabinovich, M.: Least-squares rigid motion using svd (2017)
26. Staring, M., Klein, S., Pluim, J.P.: A rigidity penalty term for nonrigid registration. *Medical physics* **34**(11), 4098–4108 (2007)
27. Tins, B.: Technical aspects of ct imaging of the spine. *Insights into imaging* **1**(5), 349–359 (2010)
28. Wells III, W.M., Viola, P., Atsumi, H., Nakajima, S., Kikinis, R.: Multi-modal volume registration by maximization of mutual information. *Medical Image Analysis* **1**(1), 35–51 (1996)